not been discussed in the Technical Note, note that it will contribute to the conical sheet instability. Further investigation of the effect of fluid swirl velocity on breakup length is required to elucidate the relationship between breakup length and both Weber and Reynolds numbers.

## Conclusions

The effect of fluid properties on the liquid sheet features, discharge coefficient, and sheet disintegration was examined experimentally with a simplex pressure-swirl atomizer. The fluid properties of viscosity and surface tension both affect the sheet features, that is, sheet surface appearance and spray cone shape. The fluid properties of viscosity, surface tension, and density affect the discharge coefficient of a pressure-swirl atomizer. For viscosity, the discharge coefficient decreases with an increase of Reynolds number, but the change is reduced significantly when the Reynolds number becomes larger than $2 \times 10^3$. When $Re > 2 \times 10^3$, both fluid density and surface tension affect the discharge coefficient.

The variation of the breakup length with Reynolds number and Ohnesorge number indicates two distinct regimes. When $Re < 2 \times 10^3$, the breakup length decreases with an increase of Reynolds number, and is independent of Ohnesorge number. Liquid viscosity is the primary factor that influences breakup in this region. When $Re > 2 \times 10^3$, both Reynolds number and Ohnesorge number affect the breakup length such that enhanced liquid inertia (via Reynolds number) reduces further the breakup length, and increased surface tension (via Ohnesorge number) enlarges breakup length. Relating breakup length to Weber and Ohnesorge numbers also supports these results with regard to the influence of liquid viscosity, surface tension, and inertia on breakup length.

## References

[1]Rizk, N. K., and Lefebvre, A. H., "Internal Flow Characteristics of Simplex Swirl Atomizers," *Journal of Propulsion and Power*, Vol. 1, No. 3, 1985, pp. 193–199.

[2]Suyari, M., and Lefebvre, A. H., "Film Thickness Measurements in a Simplex Swirl Atomizer," *Journal of Propulsion and Power*, Vol. 2, No. 6, 1986, pp. 528–533.

[3]Wang, X. F., and Lefebvre, A. H., "Mean Drop Sizes from Pressure-Swirl Nozzles," *Journal of Propulsion and Power*, Vol. 3, No. 1, 1987, pp. 11–18.

[4]Squire, H. B., "Investigation of the Instability of a Moving Liquid Film," *British Journal of Applied Physics*, Vol. 4, June 1953, pp. 167–169.

[5]York, J. L., Stubbs, H. E., and Tek, M. R., "The Mechanism of Disintegration of Liquid Sheets," *Transactions of the American Society of Mechanical Engineers*, Vol. 75, Oct. 1953, pp. 1279–1286.

[6]Hagerty, W. W., and Shea, J. F., "A Study of the Stability of Plane Fluid Sheets," *Journal of Applied Mechanics*, Vol. 22, Dec. 1955, pp. 509–514.

[7]Clark, C. J., and Dombrowski, N., "Aerodynamic Instability and Disintegration of Inviscid Liquid Sheets," *Proceedings of the Royal Society of London, Series A: Mathematical and Physical Sciences*, Vol. 329, No. 1579, 1972 pp. 467–478.

[8]Rangel, R. H., and Sirignano, W. A., "The Linear and Nonlinear Shear Instability of a Fluid Sheet," *Physics of Fluids A*, Vol. 3, No. 10, 1991, pp. 2392–2400.

[9]Lin, S. P., "Stability of a Viscous Liquid Curtain," *Journal of Fluid Mechanics*, Vol. 104, March 1981, pp. 111–118.

[10]Li, X., and Tankin, R. S., "On the Temporal Instability of a Two-Dimensional Viscous Liquid Sheet," *Journal of Fluid Mechanics*, Vol. 226, May 1991, pp. 425–443.

[11]Dombrowski, N., and Fraser, R. P., "A Photographic Investigation into the Disintegration of Liquid Sheets," *Philosophical Transactions of the Royal Society of London, Series A: Mathematical and Physical Sciences*, Vol. 247, Sept. 1954, pp. 101–130.

[12]Rizk, N. K., and Lefebvre, A. H., "Influence of Liquid Film Thickness on Airblast Atomization," *Journal of Engineering for Power*, Vol. 102, No. 3, 1980, pp. 706–710.

[13]Lefebvre, A. H., *Atomization and Sprays*, Hemisphere, New York, 1989, pp. 112–117.

[14]Fraser, R. P., "Liquid Fuel Atomization," *Sixth Symposium (International) on Combustion*, Reinhold, New York, 1957, pp. 687–701.

[15]Chung, I. P., Presser, C., and Dressler, J. L., "The Effect of Piezoelectric Transducer Modulation on Liquid Sheet Disintegration," *Atomization and Sprays*, Vol. 8, No. 5, 1998, pp. 479–502.

[16]Radcliffe, A., "The Performance of a Type of Swirl Atomizer," *Proceedings of the Institution of Mechanical Engineers*, Vol. 169, No. 3, 1955, pp. 93–106.

# Characteristic Gap: A New Design Criterion for Solid Rocket Motors

Daniel Chasman*
*Tensor Aeronautics, San Ramon, California 94583-1948*

## Introduction

THIS Note reports on development of a new, more straightforward relationship between certain solid rocket motor geometric properties and the predicted pressure spike. The values of this theoretical relationship agree well with experimental data. It also demonstrates how to apply the relationship to motor design methods.

Internal ballistics formulations developed for the design of solid rocket motors (SRM) are derived from the conservative equations using either the differential or the integral form.[1–7] The latter method is more convenient because control volume selection for the internal aerodynamics is defined by the motor geometry. It is also easier to identify the origin of terms, that is, steady-state vs unsteady terms, and, thus, to keep them separated. Because the substantial derivative is decomposed into temporal and spatial terms, it is easier to monitor the mathematical rigor of the equations of motion and to apply physically meaningful simplifying assumptions to convective terms alone or to temporal terms alone. We follow the same procedure in the present study to obtain unsteady equilibrium.

Before ignition, the pressure in the chamber is ambient. As the propellant is ignited, it generates hot gas, which fills the void volume of the chamber and pressurizes it to the design pressure in the chamber, and then the gas is ejected through the nozzle. In cases where a burnt gas mass is generated in an increasingly small void volume, the chamber fills too fast, which causes a higher than designed pressure in the chamber. For propellants with pressure-dependent burn rates, such conditions create a feedback loop process that forces ever higher generated mass, which cannot be ejected at the rate of production and, thus, is stored. For a volume that is too large, on the other hand, the same given generated mass is not sufficient to pressurize the chamber to the designed pressure level. In extreme cases, the rocket motor is extinguished prematurely.

When a thrust requirement forces designers to pack more grain in a given volume to increase the mass fraction (initial to final mass of an SRM,[1–3] usually both nozzle efficiency and void volume are sacrificed. Such a design constraint applies to all sizes of SRMs, but is more dramatic in small SRMs. This constraint sets the conditions for a nonequilibrium, erosively burning motor. The main concern, then, shifts from the choice between balanced vs nonbalanced design to that of solving of the problem of how to minimize and/or predict the pressure spike in the chamber. This is an important issue not only for the motor performance but also for the case material selection, the wall thickness, and for the design safety margin. When a multinozzle design is selected, a further reduction of the void volume, otherwise available in the convergent cone of a single-nozzle design, occurs. Although this is the reason why multinozzle design improves the mass fraction, it is also what increases sensitivity to erosive burning and, thus, to pressure spike.

The present study first discusses the theoretical aspects of the concept, which follows a previous development of an unsteady-state equilibrium formulation[4] to develop a modified unsteady-state equilibrium formulation that leads to a new design criterion. Next, experimental data corroborate the theory and demonstrate its physical interpretation. The data also demonstrate how to apply the equation to motor design.

Received 26 June 1998; revision received 21 February 2000; accepted for publication 17 March 2000. Copyright © 2000 by the American Institute of Aeronautics and Astronautics, Inc. All rights reserved.

*Senior Scientist, Propulsion, 2862 Bollinger Canyon Road. Senior Member AIAA.

## Theoretical Background

By the use of the continuity equation in the integral form in a similar fashion to that shown by Barrere et al. (Ref. 4, page 238), the following equation was developed:

$$V_c \cdot \frac{\Delta p_c}{p_c \cdot \Delta t} + \frac{A_b \cdot \dot{r} \cdot \Delta t}{\Delta t} = \frac{\rho_p}{\rho_g} \cdot \dot{r} \cdot A_b - \frac{p_c}{\rho_g} \cdot A_t / C^* \qquad (1)$$

where $V_c$ is the chamber void volume, $p$ is the pressure, $\rho$ is the density, $\dot{r}$ is the burn rate, $C^*$ is the characteristic exhaust velocity, and $A_t$ and $A_b$ are the throat area and the propellant burning area, respectively.

Unlike Barrere et al.,[4] who regrouped the two mass flow (unsteady and steady state, respectively) terms containing $\dot{r}A_b$, we obey the substantial derivative decomposition rule. Thus, we keep the unsteady terms on one side of the equation so that unsteady equilibrium conditions can be derived properly. Dividing Eq. (1) by $\dot{r}A_b$ and canceling $\Delta t$, we obtain

$$\frac{V_c}{A_b} \cdot \frac{\Delta p_c}{\dot{r} \cdot p_c \cdot \Delta t} + 1 = \frac{\rho_p}{\rho_g} - \frac{p_c}{\rho_g \cdot \dot{r} \cdot C^* \cdot A_b / A_t} \qquad (2)$$

Letting both sides approach zero yields the desired equilibrium conditions. The steady-state condition, that is, the right-hand side of Eq. (2), was similarly obtained elsewhere.[1–7] After $\Delta P_c$ is defined as the delta between the designed pressure in the chamber and the pressure spike, that is, $\Delta P_c = P_c - P_{\text{spike}}$, and $\Delta P^*$ as the dimensionless term $(\Delta P_c / P_c)$, the unsteady equilibrium condition can be defined as

$$1 - \frac{V_c}{A_b} \cdot \frac{p_{\text{spike}} - p_c}{\dot{r} \cdot p_c \cdot \Delta t} = 0 \qquad \text{or} \qquad 1 = \frac{V_c}{A_b} \cdot \frac{\Delta p^*}{\dot{r} \cdot \Delta t} \qquad (3)$$

The void volume can be defined by the burning surface area times a length that in some cases can match the gap between the propellant burning surface and the nozzle throat. This distance $X$ is called the characteristic gap and is the product of dividing the void volume by the burn surface area. After rearranging terms, the final unsteady equilibrium ratio assumes the form

$$\dot{r} \Delta t / X = (p_{\text{spike}} / p_c - 1) \qquad (4)$$

where $\Delta t$ is timescale of the given transient.

The characteristic length of the motor $L^*$ has been used in solid motor design for several decades. According to Kruse,[7] this length defines the residence time of a rocket motor. The geometric characteristic length $L^*_{\text{geo}}$, on the other hand, defines a purely geometric ratio. The characteristic gap $X$ can be related accordingly as

$$X = \frac{V_c}{A_b} \equiv \frac{V_c / A_t}{A_b / A_t} = \frac{L^*_{\text{geo}}}{K_n} \qquad \text{or} \qquad K_n = f\left(\frac{1}{X}\right) \qquad (5)$$

Because $K_n$ is a steady equilibrium ratio, Eq. (5) demonstrates the interdependency of the steady- and the unsteady-state equilibrium criteria. Once the restriction ratio $K_n$ is selected and $P_c$, $A_b$, $A_t$, and the grain geometry are derived using the first criterion, then the minimal void volume is obtained based on the same $K_n$, the desired pressure spike, the time $\Delta t$ it takes to reach it, and the burn rate. The restriction ratio $K_n$ can be redefined using Eq. (5) as a function of the characteristic gap $X$. This relationship, shown in Fig. 1, between the steady-state equilibrium parameter $K_n$ and the unsteady-state equilibrium parameter $X$ is characteristic of series hyperbolas that depend on the value of $L^*_{\text{geo}}$. This can easily be shown in a void volume with constant burn area such as that of an end-burning motor, where the dominant parameter defining this volume is $X$. For a small $X$ and a small $V_c$, the initially generated mass of hot gas pressurizes the chamber to a higher pressure peak than that of a larger $X$. Figure 1 shows these trends qualitatively: The numbers change from one propellant grain composition to the next and from one chamber geometry to another. Figure 1 represents propellant compositions that are hard to start. For propellant compositions with slow burn rate, that is, Mg/PTFE (a magnesium and Teflon® mix), detonation or extinguishment may not occur. Mg/PTFE may experience combustion instability due to high void volume (or characteristic gap), but continues to burn at ambient conditions.

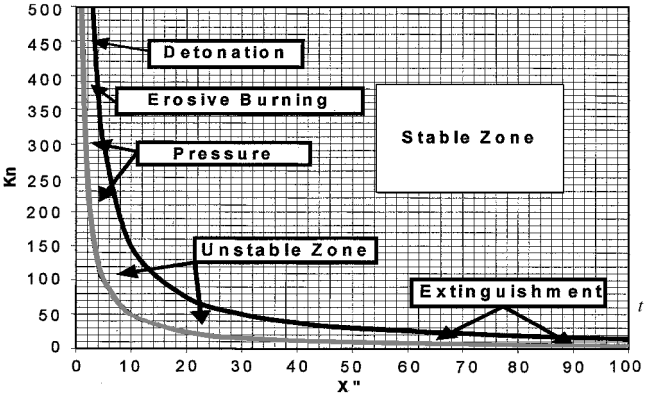


**Fig. 1 SRM chamber equilibrium conditions.**

## Experimental Test Methods

Two development programs, designed, developed, and tested onsite, were selected from a repertoire of small rocket motors and kinematic decoys. These motors represent grains with a mass that is less than a pound and mass fraction of about 0.7. The grain geometry was not an end-burn type, but was rather a complex finger shape with internal groove and inhibited external surfaces. Both decoys employed multinozzle geometry, which increases the sensitivity to pressure spike. The tests were conducted using a pressure vessel (bomb test apparatus type) with a pressure tap. The pressure transducer was quartz load cell with a builtin amplifier. This sensor had a sensitivity of $1 \pm 0.1$ mv/psi (i.e., millivolt/psi) and a resolution of 0.1 psi with dynamic range of 1–5000 psi. The sampling rate used was 2000 Hz.

## Experimental Test Results

Figure 2 shows pressure plots of experimental data from static testing of the larger decoy. The pressure histories correlate with the tail gap, which was measured before each of the firings. The tail gap represents the distance (in inches) from the internal surface of the nozzle plate to the tail face of the grain. The void volume of this configuration consists of three main contributors: the complex, fingerlike port volume (constant) of the grain; the multinozzle convergent cones (negligible); and the volume formed by the gap defined earlier (variable). The gap varied as a result of manufacturing tolerances. Before controlling and defining this tolerance, the gap varied as a function of amount of adhesive, inhibitor, and the strength of the operator who pushed the grain toward the nozzle plate. X-ray photography, combined with direct measurements from the nozzle plate, provided the actual gap measurement.

Figure 3 shows the data from the two programs reported. The first set of data represents the larger decoy. The value of $\Delta t$ (0.06 s) represents the pressure rise time from zero to spike. The burn-rate value of 0.59 in./s represents the mean value from several tests. The next set of data represents a motor that is about a quarter of the first in size (both diameter and length are different) with a $\Delta t$ value of 0.09 s and a burn-rate value of 0.259 in./s. More experimental data were available for this program.

The experimental $X$ data points were obtained, dividing the measured void volume $V_c$ by the measured burn surface $A_b$. The experimental values of $\Delta P^*$ were obtained by subtracting 1 from the ratio of the measured pressure spike to chamber pressure. The theoretical curves are based on Eq. (4). Whereas the constants were obtained when the measured burn-rate values were multiplied by that of the rise time, the theoretical $X$ data points were selected arbitrarily to cover the range of the experimental data and, then, to determine the $\Delta P^*$ values. Knowing the chamber pressure yields the pressure spike. Figure 3 also shows that the correlation between the theoretical and the experimental is quite consistent. Also noticeable is the sensitivity of the smaller motor to pressure spike (experimental data points have lower values for higher values of spike-to-chamber

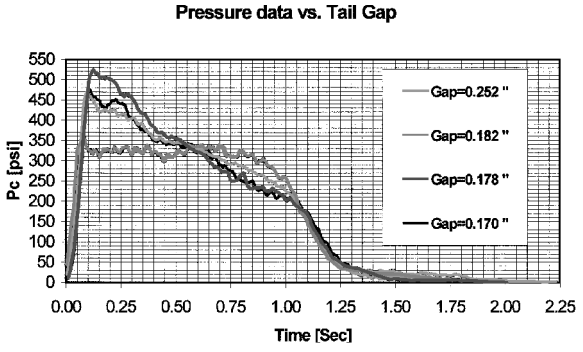


**Fig. 2 Static test results of pressure histories vs the tail gap.**

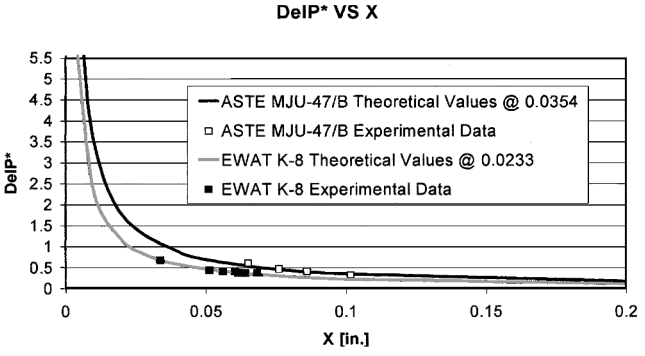


**Fig. 3 Pressure ratio $\Delta P^*$ vs $X$: experimental vs theoretical data.**

ratio, which indicates higher values of pressure spike for smaller $X$ values). These findings show that Eq. (4) provides a reasonable prediction of the pressure spike value once the burn rate and the rise time are known.

## Discussion

Variational principles[8] dictate that for equilibrium conditions to occur both sides of Eq. (2) should vanish. Keeping steady-state terms separated from the unsteady terms enables separate equilibrium conditions for each of these states. This seems not only mathematically correct but also true to the physical meaning of the substantial derivative decomposition procedure in the mass flow balance. The geometric characteristic length, which defines the ratio between the void volume and the throat area, was obtained[4] by mixing steady and unsteady terms. In contrast, the physical interpretation of the new equilibrium conditions is that, when the throat area is changed, new steady-state conditions and performance occur, and thus the stage is set for different unsteady-state equilibrium conditions. In the presented experimental tests, the throat area remained unchanged, but pressure spikes occurred (see Fig. 2) as the $X$ changed. Furthermore, the two motors reported in this study with different port area and case diameter showed that variations in $X$ correlated well with the pressure spike. Finally, note [Eq. (5)] that the connecting term between the purely unsteady condition, $X$, and the purely steady condition, $K_n$, is the geometric characteristic length $L^*$, which was originally derived from mixed terms.

## Conclusions

A new design criterion for unsteady equilibrium in SRM was derived from the conservative mass balance equation in integral form. This relation [Eq. (4)] shows the dependency not only of the pressure spike on grain properties (such as burn rate and rise time) but also on a geometric parameter called the characteristic gap. The characteristic gap $X$ defines the ratio between the void volume and the propellant burning surface. In basic motor design, it is sometimes close in dimension to the physical gap between the throat and the end-grain surface. The new unsteady-state equilibrium was corroborated with the experimental data and was found to work consistently as a design tool to predict pressure spikes early in the design.

More experimental testing is suggested. The correlation between the $X$ and the pressure spike should be clearly demonstrated in an end-burning-type test apparatus. In contrast to SRMs with complex grain geometry, end-burning-type test setups will enable visual verification of the relationship between the SRM geometric parameters and the design criteria of equilibrium conditions.

## Acknowledgment

The research reported in this Note was funded in part by the ASIE program, Wright–Patterson AFB, Ohio 45433-7017, Contract no. 33657-95-C-0006.

## References

[1] Sutton, G. P., *Rocket Propulsion Elements*, 6th ed., Wiley, New York, 1992, Sec. 11.2, p. 384.

[2] Zucrow, M. J., *Aircraft and Missile Propulsion*, Vol. 1, Wiley, New York, 1958, pp. 91, 92.

[3] Zucrow, M. J., *Aircraft and Missile Propulsion*, Vol. 2, Wiley, New York, 1958, pp. 419–433.

[4] Barrere, M., Jaumotte, A., De Veubeke, B. F., and Vandenkerchove, J., *Rocket Propulsion*, Elsvier, New York, 1960, pp. 237–247.

[5] Hill, P. G., and Peterson, C. P., *Mechanics and Thermodynamics of Propulsion*, Addison Wesley Longman, Reading, MA, 1987, pp. 117–119.

[6] Brooks, W. T., Workshop Report: Burn Rate Determination Methodology, CPIA Publ. 347, Vol. 2, Chemical Propulsion Information Agency, Columbia, MD, Oct. 1981, pp. 183–191.

[7] Kruse, R. B., *Fundamental of Solid Rocket Motors*, Univ. of Huntsville Press, Huntsville, AL, 1991, p. 27.

[8] Yourgrau, W., and Mandelstam, S., *Variational Principles in Dynamics and Quantum Theory*, Dover, New York, 1979, Sec. 4, pp. 145–152.

# Concentration Measurements in a Mixing Module for Lean, Premixed, Gas-Turbine Combustors

D. Douglas Thomsen,* R. V. Ravikrishna,†
Clayton S. Cooper,* Yanan Jiang,§
and Normand M. Laurendeau¶
*Purdue University, West Lafayette, Indiana 47907-1288*

## Introduction

RECENT government emission standards mandating low $NO_x$ levels in advanced gas-turbine engines have led to the use of lean, premixed combustion.[1] Lean, premixed combustion reduces thermal $NO_x$ by preventing the creation of the high-temperature, stoichiometric interfaces found in traditional diffusion flames. However, the advantages of this technique depend upon the flame burning at the same lean equivalence ratio at all locations and times. The exponential dependence of $NO_x$ on temperature causes relatively small spatial or temporal variations in equivalence ratio to produce substantial increases in $NO_x$ emissions.[2] Thus, mixing efficiency is a critical property of any proposed lean-premixed combustor.

One proposed design for achieving the goal of well-mixed lean combustion for natural gas applications, while minimizing the

Received 28 February 1999; revision received 5 January 2000; accepted for publication 25 February 2000. Copyright © 2000 by the authors. Published by the American Institute of Aeronautics and Astronautics, Inc., with permission.

*Researcher; currently Combustion Design Engineer, Advanced Combustion Engineering, General Electric Aircraft Engines, Cincinnati, OH.

†Researcher; currently Assistant Professor, Department of Mechanical Engineering, Indian Institute of Science, Bangalore, India.

§Research Associate, Department of Chemistry.

¶Reilly Professor of Combustion; currently Ralph and Bettye Bailey Professor of Combustion.